IEEE Access
Multidisciplinary | Rapid Review | Open Access Journal

Received January 31, 2021, accepted February 8, 2021, date of publication February 11, 2021, date of current version February 25, 2021.

Digital Object Identifier 10.1109/ACCESS.2021.3058521

Optimum Modified Fractional Order Controller for Future Electric Vehicles and Renewable Energy-Based Interconnected Power Systems

EMAD M. AHMED[1,2], (Senior Member, IEEE), EMAD A. MOHAMED[2], AHMED ELMELEGI[2], MOKHTAR ALY[2,3], (Member, IEEE), AND OSAMA ELBAKSAWI[1,4]

[1]Department of Electrical Engineering, College of Engineering, Jouf University, Sakaka 2014, Saudi Arabia
[2]Department of Electrical Engineering, Faculty of Engineering, Aswan University, Aswan 81542, Egypt
[3]Electronics Engineering Department, Universidad Técnica Federico Santa María, Valparaiso 2390123, Chile
[4]Department of Electrical Engineering, Faculty of Engineering, Port Said University, Port Fuad 42526, Egypt

Corresponding author: Emad A. Mohamed (emad.younis@aswu.edu.eg)

The authors extend their appreciation to the Deputyship for Research Innovation, Ministry of Education in Saudi Arabia for funding this work through the project number ''375213500''. The authors also would like to extend their sincere appreciation to the central laboratory at Jouf University for support this study. This work is also supported in part by SERC Chile (ANID/FONDAP15110019) and by AC3E(ANID/Basal/FB0008).

ABSTRACT Several issues have been risen due to the recent vast installations of renewable energy sources (RESs) instead of fossil fuel sources in addition to the replacement of electric vehicles (EVs) for fuel-powered vehicles. Mitigating frequency deviations and tie-line power fluctuations has become driving challenge for the control design of interconnected power systems. RESs represent continuously varying power generators due to their nature and dependency on the environmental conditions. In this context, this article presents a new modified hybrid fractional order controller for load frequency and EVs control in interconnected power systems. The new controller combines the benefits of two widely employed fractional order controllers, including the FOPID and TID controllers. In addition, a new practical application of recent artificial ecosystem optimization (AEO) method has been proposed in this article for determining simultaneously the optimum controller parameters. The proposed controller and optimization method are validated on two areas interconnected power system with different types of RESs and with considering the natural characteristics of sources, EVs and load variations. Obtained simulation results verify the superior performance of the proposed controller and optimization method for achieving high mitigation of frequency fluctuations and tie-line power deviations, increased robustness, enhanced system stability over a wide range of parameters uncertainty and fast response during transients.

INDEX TERMS Artificial ecosystem optimization, electric vehicles (EVs), fractional order controller, load frequency control, renewable energy sources.

I. INTRODUCTION

With the increased deployment of renewable energies, modern power systems have encountered several challenges regarding system design, operation, and control [1], [2]. The necessity to find out new controllers with capabilities of damping out system oscillations has become an important issue, in particular with the targeted high penetration levels of the renewable energies [3]. Besides, special considerations are required to properly design, control and manage future power systems that are highly penetrated with renewable energy sources (RESs) [4]. The intermittent feature of the photovoltaic (PV) and wind energies has forced the power system to have different technologies and strategies to be more flexible and proficient for compensating the load/generation variations. Therefore, the energy storage systems (ESSs) are included inherently to overcome such power unbalance and frequency deviation problems in order to keep system stability [5]–[7]. Thence, ESSs are considered as the most essential element in modern power systems since they can act instantaneously to tackle any power unbalance or load variations.

The power system models are equipped with different control loops, such as primary, secondary, and

The associate editor coordinating the review of this manuscript and approving it for publication was Chandan Kumar.

tertiary control systems [8]. Both the primary and secondary control loops are responsible for regulating and recovering system frequency. The primary control loop is used to damp out the small changes in frequency deviations in the normal operation [9]. However, for larger frequency deviations, the secondary control loop, which is known as the Load frequency control (LFC), is used to regulate area frequency to the original conditions and maintain the scheduled tie-line power in the power systems according to the power reserve [10]. Recently, with the increased use of electrical vehicles (EVs), the conception of the vehicle to grid (V2G) has appeared. In which, EV batteries are used to decouple system generations and load demands, especially when the renewable energy sources are not generating their expected powers [11]. Therefore, by properly controlling the EV batteries using grid-connected bi-directional converters, the EV batteries are allowed to charge/discharge to support the load changes and adjust the grid frequency [12].

A. LITERATURE REVIEW

In the literature, there are several research proposals for including the EVs in the LFC [13], [14]. However, the complexity of controlling EVs with the existing LFC methods has become challenging issue, especially with interconnected multi-area power systems. There are numerous proposed optimized controllers for LFC in the literature using the integral order, fractional order (FO), fuzzy logic controller (FLC), neural network (NN), model predictive control (MPC) and intelligent control systems [15]–[17]. The various control elements using proportional (P), integrator (I), derivative (D), tilt (T) and derivative filter (F) have been widely combined in the literature for developing various LFC systems. The PI controller has been presented in [18] for EVs. However, this controller exhibited stability issues, especially when considering the time delays of the communication system. The FOPID with FO filter has been proposed in [19] and it has been optimized using the sine–cosine optimizer algorithm (SCA). The PID controller has been designed using the stability boundary-locus (SBL) method in [20]. In [21], the parameters for PI LFC have been optimally designed using the Harris Hawks Optimization (HHO) algorithm. The control of EVs using TID controllers and being optimized by the artificial-bee-colony optimizer (ABC) has been proposed in [22]. Additional, optimized AGC method has been presented in [23] based on the full-state feedback control theory for interconnected power systems. An enhanced performance is obtained in comparison with GA-tuned control methods. Moreover, the particle swarm optimizer algorithm (PSO) has been applied for designing the virtual inertia control system in [24]. In [25], an improved FFOID controller has been presented with ultra-capacitor energy storage device for solving the AGC issues in interconnected power systems. Also, an optimized design for the TID controller has been presented using the pathfinder optimization algorithm (PFA) [26].

In [27], the FOPID is cascaded with FLC for achieving frequency regulation in two-area power systems. The imperialist competitive optimizer algorithm (ICA) has been introduced for optimizing controller parameters. The adaptive PI control has been proposed in [28] for coordinating EVs to achieve regulated frequency of the microgrids. The application of the cascaded controllers with the ICA optimizer for controlling EVs has been presented in [29]. In [30], an improved controller based on ICA-optimized FPIDN-FOPIDN controller has been proposed for AGC in two-area power systems. The presented controller can effectively enhance the performance of power systems at various step changes in the generation and/or loading. In [31], the design of adaptive integrator-based LFC has been presented using the electro-search optimizer (ESO) and the balloon effect modulation (BE). The utilization of BE with the standard ESO method has resulted in increasing the ability of the controller to reject load disturbances and parameter changes. Additionally, the improved fitness dependent optimization method (I-FDO) has been proposed for designing the FOI-PD controller in two-area power systems [32]. Another application of ICA optimizer has been proposed in [33] for determining the optimal parameters for the new FTIDF-II controller for AGC systems.

Modified controllers have been also proposed in the literature for LFC. Modified TID controller with filter (TIDF) optimized with the differential evolution optimization (DE) method has been presented in [34]. The slap swarm optimizer algorithm (SSA) was proposed in [35] for tuning the PI-TDF controller. Additionally, the butterfly optimizer algorithm (BOA) has been presented for designing the dual-stage PI-(1+ID) controller in [36]. The hybrid FO controller has been presented and optimized using manta ray foraging optimizer algorithm (MRFO) in [37]. A novel cascaded FO-ID with filter ($C - I^{\lambda}D^{\mu}N$) controller has been proposed in [38] for AGC systems in power systems with solar, fuel cell, and wind generators.

From another side, optimized modern controllers have been presented in the literature for LFC applications. The sooty terns optimizer algorithm (STOA) has been introduced in [39] for optimizing the MPC in LFC systems. Further, multi-verse optimization (MVO) based MPC controller has been proposed in [40]. The ABC optimizer-based terminal siding-more controller (TSMC) has been presented for LFC in [41]. The full SMC has been proposed for LFC that combines the TSMC and linear SMC (LSMC) methods in [42]. However, these methods require accurate and complex mathematical models for power systems. Optimized design for FLC systems for EVs in multi-area power systems has been presented in [43] using the ICA optimizer. Another adaptive droop controller with the fuzzy-PI controller has been optimized using the genetic algorithm optimizer (GA) [44]. A modified fuzzy-PID controller optimized with the tribe-DE optimizer (TDE) has been introduced in [45].

B. RESEARCH GAP AND MOTIVATION

The above-mentioned controllers and their design process emphasize the issues for selecting and designing the LFC

and EVs controllers, especially when considering the behavior of RESs, loads and EVs [37]. It can be also seen that FO-based controllers provide several superiority points in frequency regulation applications. They provide simple, robust and efficient solutions. Moreover, the design of multiple FO controllers in each interconnected power system represents an additional issue for LFC and EV control [19]. Therefore, this article presents a modified FO-based controller for LFC and EV control in two-area interconnected RES and EV-based power systems. Furthermore, the recent efficient artificial ecosystem optimization (AEO) has been applied for the first time, thanks to the authors knowledge, for designing LFC and EV controllers.

C. CONTRIBUTION AND PAPER ORGANIZATION

Accordingly, the major contributions of this article can be summarized as follows:

- A modified fractional order-based controller is proposed for both LFC and EVs to fully mitigate frequency fluctuations and tie-line power deviations. The proposed controller represents a new combination of the benefits of two widely utilized FOPID and TID controllers.
- An improved utilization of future EVs is presented to contribute in frequency regulation and enhancing power system performance. The installed EVs are employed to contribute in the LFC functionalities in this article.
- A new practical application for the newly developed AEO method is proposed for optimizing the parameters of the proposed controllers simultaneously. The benefits of recent AEO algorithm are combined with the proposed method to provide robust and stable control of the power systems.
- A cooperative share between LFC and EVs for regulating the tie-line power and regulating frequency for the interconnected power systems is introduced. The proposed controller improves the coordination between the installed EVs and LFC devices in the studied power system.

The remaining of the article is organized as follows: Section II provides the mathematical model for power system components in addition to EV models for frequency regulation. Section III introduces the new proposed controller. Section IV details the AEO method and the optimizations problem. The results and discussion of the studied case are provided in Section V. Conclusion of the article is provided in Section VI.

II. MODELLING OF POWER SYSTEM ELEMENTS

A. EV MODELLING

In order to explore the impact of the EVs on the LFC, the EV model is required to count for its internal characterstics. In the studied system, two stations of EV are considered as ESSs to cooperate with LFC to mitigate the imbalance of load demand and generation. In Fig. 1, an accurate dynamic model of the EV is developed, where its detailed electrical equivalent circuit is presented in [43], [46]. The Thevenin equivalent

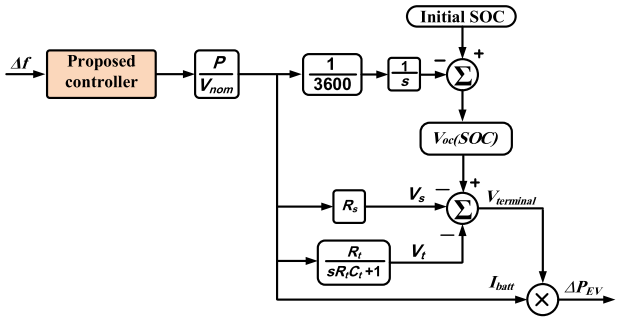

FIGURE 1. Modelling of EV for LFC studies.

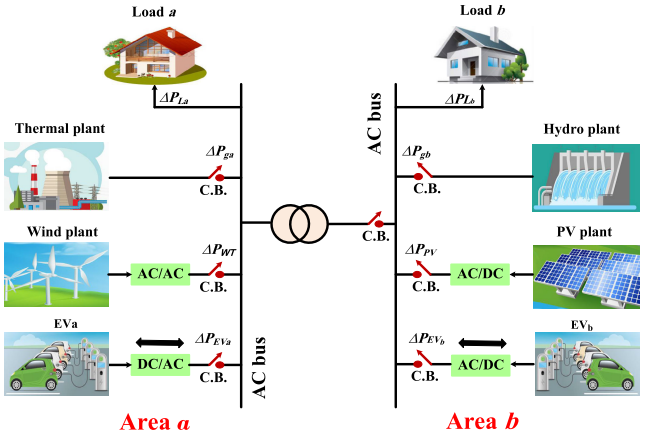

FIGURE 2. Overall diagram of the studied two-area power system.

EV model is adopted. It consists of an open circuit voltage source, which is being a function in the initial battery state of charge (SOC), connected in series with a series resistance R_s and a parallel RC branch (R_t, C_t), which describes the transient over-voltage effect. The terminal EV voltage is obtained by combining the open-circuit voltage and the voltage drop across the series resistance and the voltage drop across the RC branch as shown in Fig. 1. Nernst equation is used to implement the relation between the V_{oc} and the SOC of EV as follows (1) [47]:

$$V_{oc}(SOC) = V_{nom} + S\,\frac{RT}{F} ln\,(\frac{SOC}{C_{nom} - SOC}) \qquad (1)$$

where $V_{oc}(SOC)$, V_{nom}, C_{nom} correspond to EV open circuit voltage as function of EV SOC, EV nominal voltage and EV nominal capacity in Ah, respectively. Whereas, S represents the sensitivity parameter between open circuit voltage and SOC of EV. In addition, F, T, R correspond to Faraday constant, temperature, and gas constant, respectively.

B. MODELLING OF GENERATION UNITS

In this article, the proposed test system comprises two-area, wherein thermal, hydro, PV and wind power plants with EV as storage system and variable types of loads disturbance are existing. Fig. 2 illustrates the overall diagram of the interconnected areas of tested electrical power system by using tie-line for exchanging power among the two-area. The block diagram of the tested interconnected two-area power

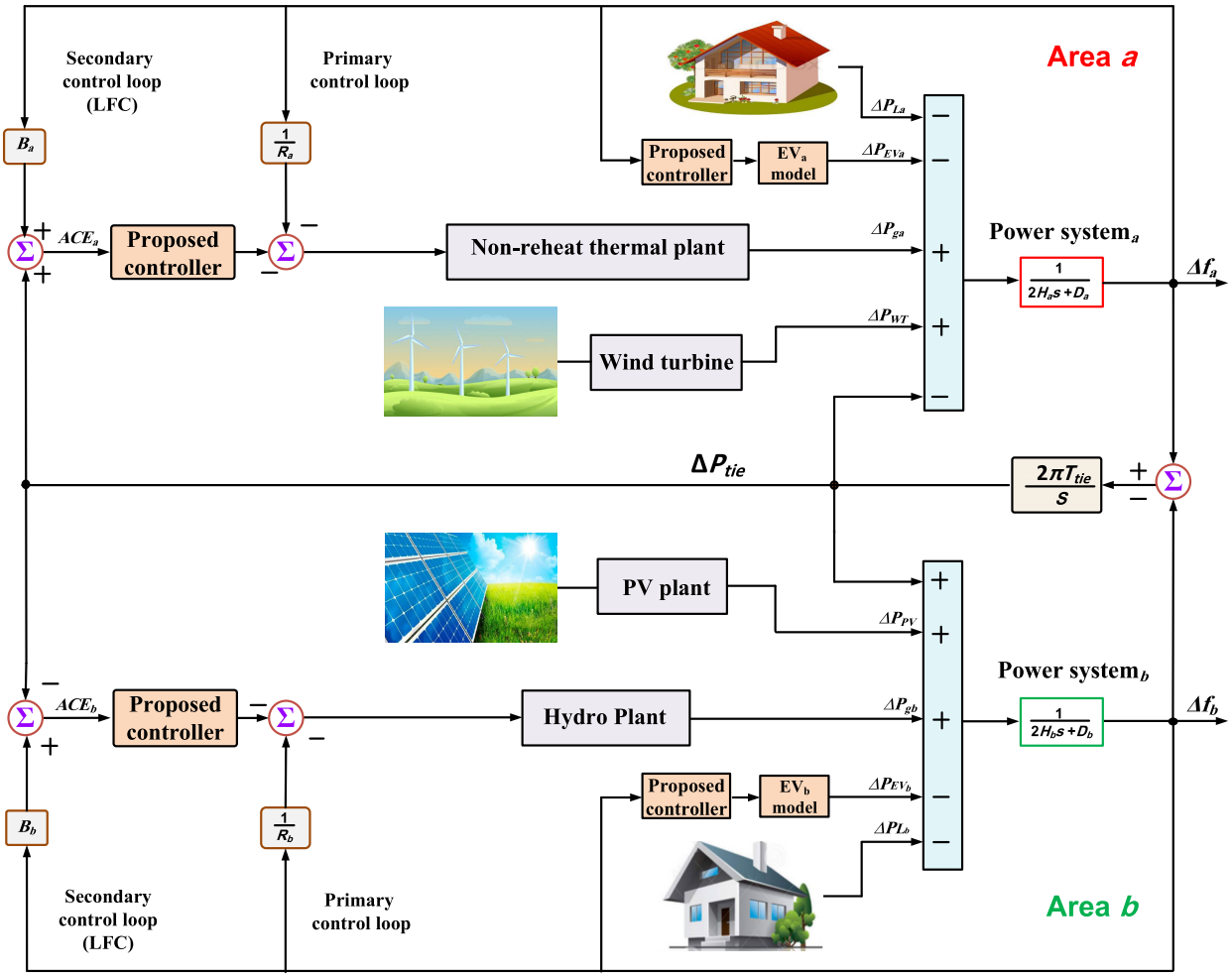

FIGURE 3. Block diagram of the tested interconnected two-area power system.

system with EVs model is shown in Fig. 3. The main parameters of the tested power system are listed in Table 1 based on the system in [37], [46].

The transfer function of the thermal generation plant is shown in Fig. 4, and it can be expressed as follows [48]:

$$G_g(s) = \frac{1}{T_g s + 1} \tag{2}$$

$$G_t(s) = \frac{1}{T_t s + 1} \tag{3}$$

where, $G_g(s)$ and $G_t(s)$ are thermal power plant governor and turbine, while T_g and T_t are governor and turbine time constants, respectively.

The transfer function of the hydraulic generation plant is shown in Fig. 5, and it can be expressed as follows [37]:

$$G_h(s) = \frac{1}{T_1 s + 1} \cdot \frac{T_R s + 1}{T_2 s + 1} \cdot \frac{-T_w s + 1}{0.5 T_w s + 1} \tag{4}$$

where T_1, T_R, T_2 are the time constants of governor, transient droop, and reset time of hydraulic governor, respectively. Whereas, T_w is starting time of water penstock.

C. MODELLING OF RESs

The transfer function of the wind generation plant can be modelled as follows [49]:

$$G_{WT}(s) = \frac{K_{WT}}{T_{WT} s + 1} \tag{5}$$

where K_{WT}, T_{WT} are the gain and time constant of wind plant, respectively. The transfer function of the PV generation plant can be expressed as follows [49]:

$$G_{PV}(s) = \frac{K_{PV}}{T_{PV} s + 1} \tag{6}$$

where K_{PV}, T_{PV} are the gain and time constant of PV plant, respectively.

III. THE PROPOSED CONTROLLER

There are numerous integral order and fractional order controllers in literature. The transfer functions for commonly used controllers can be modelled as follows:

$$C_{PI}(s) = \frac{Y(s)}{E(s)} = K_p + \frac{K_i}{s}$$

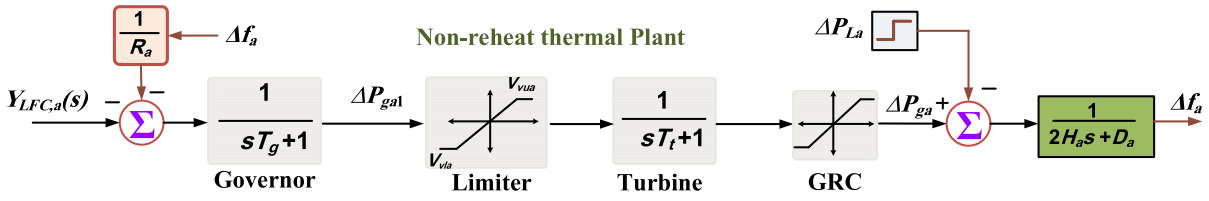

FIGURE 4. Transfer function of non-reheat thermal plant model.

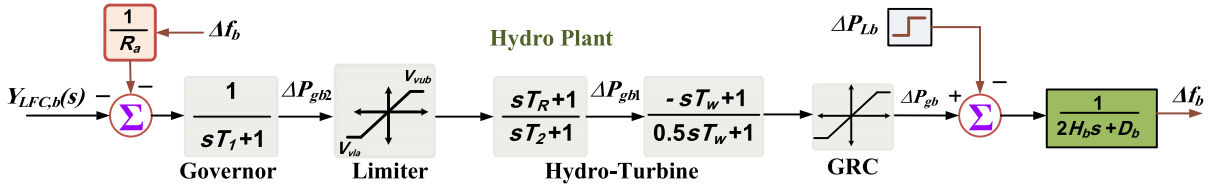

FIGURE 5. Transfer function of hydro plant model.

TABLE 1. Studied System Parameters With ($x \in \{a, b\}$).

Parameter	Symbol	Values	
		Area a	Area b
Power system parameters			
Capacity of each area	P_{rx} (MW)	1200	1200
Power system inertia constant	H_x (p.u.s)	0.0833	0.0833
Power system damping coefficient	D_x (p.u./Hz)	0.00833	0.00833
Capacity ratio gain	A_{ab}	-1	
Tie-line coefficient	T_{tie} (s)	0.0865	
LFC model parameters			
Droop constant	R_x (Hz/MW)	2.4	2.4
Frequency bias value	B_x (MW/Hz)	0.4249	0.4249
Generation power plants parameters			
Min. valve gate limit	V_{vlx} (p.u.MW)	-0.5	-0.5
Max. valve gate limit	V_{vux} (p.u.MW)	0.5	0.5
TC for thermal governor	T_g (s)	0.08	-
TC for thermal turbine	T_t (s)	0.3	-
TC for hydraulic governor	T_1 (s)	-	41.6
TC for transient droop hydraulic	T_2 (s)	-	0.513
Reset time of hydraulic governor	T_R (s)	-	5
Time of Water starting	T_w (s)	-	1
TC for PV	T_{PV} (s)	-	1.3
PV gain	K_{PV} (s)	-	1
TC for Wind	T_{WT} (s)	1.5	-
Wind gain	K_{WT} (s)	1	-
EV model parameters			
Penetration level	-	5-10%	5-10%
Nominal voltage	V_{nom} (V)	364.8	364.8
Nominal battery capacity	C_{nom} (Ah)	66.2	66.2
Series resistance	R_s (Ω)	0.074	0.074
Transient resistance	R_t (Ω)	0.047	0.047
Transient capacitance	C_t (F)	703.6	703.6
Constant values	RT/F	0.02612	0.02612
Maximum limit SOC of Battery	in %	95	95
Energy capacity of battery	C_{batt}(kWh)	24.15	24.15

* TC denotes to time constant

$$C_{PID}(s) = \frac{Y(s)}{E(s)} = K_p + \frac{K_i}{s} + K_d\ s$$
$$C_{FOPI}(s) = \frac{Y(s)}{E(s)} = K_p + \frac{K_i}{s^{\lambda}}$$
$$C_{FOPID}(s) = \frac{Y(s)}{E(s)} = K_p + \frac{K_i}{s^{\lambda}} + K_d\ s^{\mu}$$
$$C_{TID}(s) = \frac{Y(s)}{E(s)} = K_t\ s^{-(\frac{1}{n})} + \frac{K_i}{s} + K_d\ s \qquad (7)$$

where, K_p is the proportional gain, K_i is the integral gain, K_d is the differential gain, λ is the FO integration operator, μ is the FO differentiation operator and n is the FO tilt operator.

The proposed modified controller is developed by combining FOPID and TID controls. The proposed modified controller can be expressed as following:

$$C_{Proposed}(s) = \frac{Y(s)}{E(s)} = K_p + K_t\ s^{-(\frac{1}{n})} + \frac{K_i}{s^{\lambda}} + K_d\ s^{\mu} \qquad (8)$$

The proposed controller benefits both features of FOPID and the TID control systems. The employment of the FOPID adds more flexibility and dealing with disturbances at wide ranges. The FOPID can handle multiple objectives at the same time for wider operating dynamic ranges in comparison with integral order PID type. Moreover, the incorporation of the tilt part provides enhanced disturbance rejection capabilities. This in turn provides enhanced robustness of the system to the parameters uncertainties.

In the proposed control, the controller is selected for controlling the LFC in addition to EVs in each area. The two controllers are managed in cooperative manner that results in the elimination of individual area frequency fluctuations and the tie-line power disturbances. Moreover, proper and effective enhancement of the system response can be achieved through optimized determination for each controller parameters. As shown above, the new proposed controller represents a combination of effective FOPID and TID controllers from literature. The modifications of the TID controller by adding the FOPID components result in the robustness and stability of the interconnected power system. In addition, it reduces the transient time in case of various disturbances. Moreover, the new proposed controller exhibits more freedom and flexibility than traditional TID control. The proposed controllers with different elements are shown in the simplified diagram in Fig. 6. Each controller contains 7 tunable parameters, which result in having 14 tunable parameters in each area and total of 28 in the studied interconnected two-area power system. In classical control design approaches, the tuning process is very complex and requires complicated mathematical models. Therefore, in the current article, the AEO efficient

optimizer method is employed for proper determinations of the different control parameters simultaneously.

IV. THE PROPOSED OPTIMIZATION PROCESS

A. ARTIFICIAL ECOSYSTEM OPTIMIZATION

Recently, the artificial ecosystem optimization algorithm (AEO) has been applied in several optimization problems [50]. The main inducing idea for the AEO method is the transfer of cord energy among the living creatures. The transition processes are achieved by three sequential stages, including the production, the consumption, and the decomposition stages. The mathematical modelling for the three processes has been introduced in [51]. The AEO is different from previously developed meta-heuristic methods through having two major phases, including the exploration and the exploitation. In [51], consumption operator was devoted for exploration phase, where random searching is satisfied for discovering entire searching space, whereas exclusion of exploitation phase is made in decomposition process. Moreover, the production process has been presented for achieving the balance within transition process among both of exploration phase and exploitation phase [52].

The implementation of AEO was presented in [51] through organized cascade structure, wherein producer and decomposer were represented by the plants, fungi and bacteria, respectively. They are represented as a single agent, whereas remaining agents were accounted like consumers. The food type is employed as classification criteria for consumers. The food types are the herbivores that represent plants-fed animals, the omnivores that represent plats in addition to other animals-fed animals, and carnivores that represent the animals only-fed animals. Using the presented hierarchy, locations of various agents are updated through the using mathematical formulation as explained below [53]:

1) THE PRODUCTION PROCESS

The producer in AEO represents worst agent within the searching agents, while the composer represents best agent. Producer agent $x_1(t+1)$ modifies its position based on the random individuals $x_r(t)$ within the problem searching space and decomposed agent $x_n(t)$ as follows [53]:

$$x_1(t+1) = (1-a)x_n(t) + dx_r(t) \tag{9}$$

where,

$$a = (1 - \frac{t}{MaxIt}) \times r_1 \tag{10}$$

$$x_r = r_2 \times (Up - Lw) + Lw \tag{11}$$

where, Up and Lw denote to the upper and the lower boundaries within searching space, respectively, r_1 and r_2 denote to random variables within [0, 1] interval, a represents weighting coefficient, t represents current iteration, and $MaxIt$ is the maximum iteration number.

2) THE CONSUMPTION PROCESS

In this stage, the consumers are fed by the producer agent or the consumer agent with lower energy level. Every class of consumers (herbivores, omnivores, or carnivores) possesses its own strategy to catch the food (which means updating its position) according to the following [53]:

1) Herbivore consumers are only fed on producers. The locations of herbivore consumers $x_i(t+1)$ are updated using only the location of producer locations $x_1(t)$ as following:

$$x_i(t+1) = x_i(t) + C[\, x_i(t) - x_1(t)] \tag{12}$$

where, C represents the consumption factor, which can be estimated using Levy flight. It is estimated as following:

$$C = \frac{1}{2}\frac{u}{v},\ u, v, \in Norm(0, 1) \tag{13}$$

2) Omnivores consumers are fed using both of producers and animals. Thence, the positions of agents are updated using producers and the random consumers with higher energy level with index (l). It can be expressed as following:

$$x_i(t+1) = x_i(t) + C[\, r_3(x_i(t) - x_1(t))] + (1 - r_3)(x_i(t) - x_l(t)) \tag{14}$$

where,

$$l = r_i(t)([\, 2i - 1]\,), : \quad i = 3, \ldots, N \tag{15}$$

3) Carnivores consumers are fed using only other animals. Thence, the positions of agents are updated using the random consumer that has higher energy level with the index l. The mathematical modelling for the location of carnivore is expressed as following:

$$x_i(t+1) = x_i(t) + C[\, (x_i(t) - x_l(t))] \tag{16}$$

where,

$$l = r_i(t)([\, 2i - 1]\,), : \quad i = 3, \ldots, N \tag{17}$$

3) THE DECOMPOSITION PROCESS

In this process, the exploitation stage is considered and the decomposer agents start to break down remaining dead agents. The mathematical modelling of this process is expressed as following:

$$x_i(t+1) = x_i(t) + D[\, ex_n(t) - hx_i(t)] \tag{18}$$

where,

$$\begin{aligned} i &= 3, \ldots, N \\ D &= 3u, \quad u \in\in Norm(0, 1) \\ e &= r_4 r_i([\, 12]\,) - 1 \\ h &= 2r_4 - 1 \end{aligned} \tag{19}$$

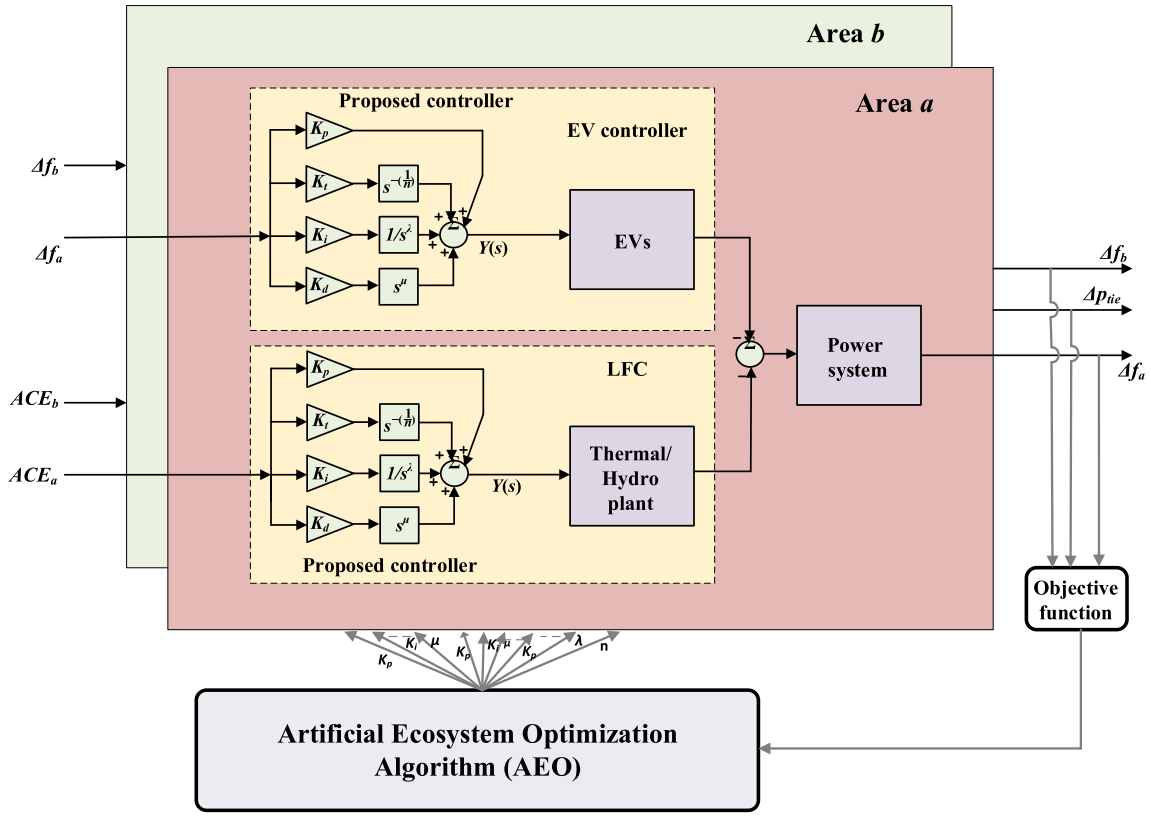

FIGURE 6. The proposed controller schematic diagram for the two-area power system.

where, D denotes to the decomposition factor, and h and e represent weighting parameters. Fig. 7 shows the flowchart of the structure of AEO algorithm to optimally determine parameters of the proposed controller.

B. OPTIMIZATION PROBLEM

In the studied system, the proposed controller has been applied to LFC and EV control functionalities in the two areas as shown in Fig. 6. The two LFC systems in addition to the two EV controllers are tuned simultaneously using the proposed AEO method. Frequency deviations of each area besides the tie-line fluctuations are employed as feedback signals to the proposed controllers. The ACE signal for areas a (ACE_a), and for area b (ACE_b) can be expressed as follows:

$$ACE_a = \Delta P_{tie} + B_a \, \Delta f_a \tag{20}$$

$$ACE_b = A_{ab} \, \Delta P_{tie} + B_b \, \Delta f_b \tag{21}$$

where, (A_{ab}) represents the capacity ratio among the two areas, and ΔP_{tie} is the tie-line power. The output of each of the proposed LFC systems can be represented as follows:

$$Y_{LFC,a}(s) = K_{p1} \, ACE_a + K_{t1} \, s^{-(\frac{1}{n_1})} \, ACE_a + \frac{K_{i1}}{s^{\lambda_1}} \, ACE_a + K_{d1} \, s^{\mu_1} \, ACE_a \tag{22}$$

$$Y_{LFC,b}(s) = K_{p2} \, ACE_b + K_{t2} \, s^{-(\frac{1}{n_2})} \, ACE_b + \frac{K_{i2}}{s^{\lambda_2}} \, ACE_b + K_{d2} \, s^{\mu_2} \, ACE_b \tag{23}$$

where, $(K_{p1}, K_{t1}, K_{i1}, K_{d1}, n_1, \lambda_1, \mu_1)$ are the controller parameters for LFC in area a. Whereas, LFC parameters for area b are $(K_{p2}, K_{t2}, K_{i2}, K_{d2}, n_2, \lambda_2, \mu_2)$. In the same way the output of EV controllers can be represented as follows:

$$Y_{EV,a}(s) = K_{p3} \, \Delta f_a + K_{t3} \, s^{-(\frac{1}{n_3})} \, \Delta f_a + \frac{K_{i3}}{s^{\lambda_3}} \, \Delta f_a + K_{d3} \, s^{\mu_3} \, \Delta f_a \tag{24}$$

$$Y_{EV,b}(s) = K_{p4} \, \Delta f_b + K_{t4} \, s^{-(\frac{1}{n_4})} \, \Delta f_b + \frac{K_{i4}}{s^{\lambda_4}} \, \Delta f_b + K_{d4} \, s^{\mu_4} \, \Delta f_b \tag{25}$$

where, $(K_{p3}, K_{t3}, K_{i3}, K_{d3}, n_3, \lambda_3, \mu_3)$ are the parameters of EV controller in area a. Whereas, EV controller parameters in area b are $(K_{p4}, K_{t4}, K_{i4}, K_{d4}, n_4, \lambda_4, \mu_4)$.

Among the various existing error-based estimations of the objective functions, the integral-squared-error (ISE) has been selected in the proposed optimization process. Compared to time integration based schemes, the ISE adds more penalization to large error values, and it can effectively reduce the peak deviations of frequency and tie-line power. The ISE is utilized for optimally determining the various parameters of the four controllers.

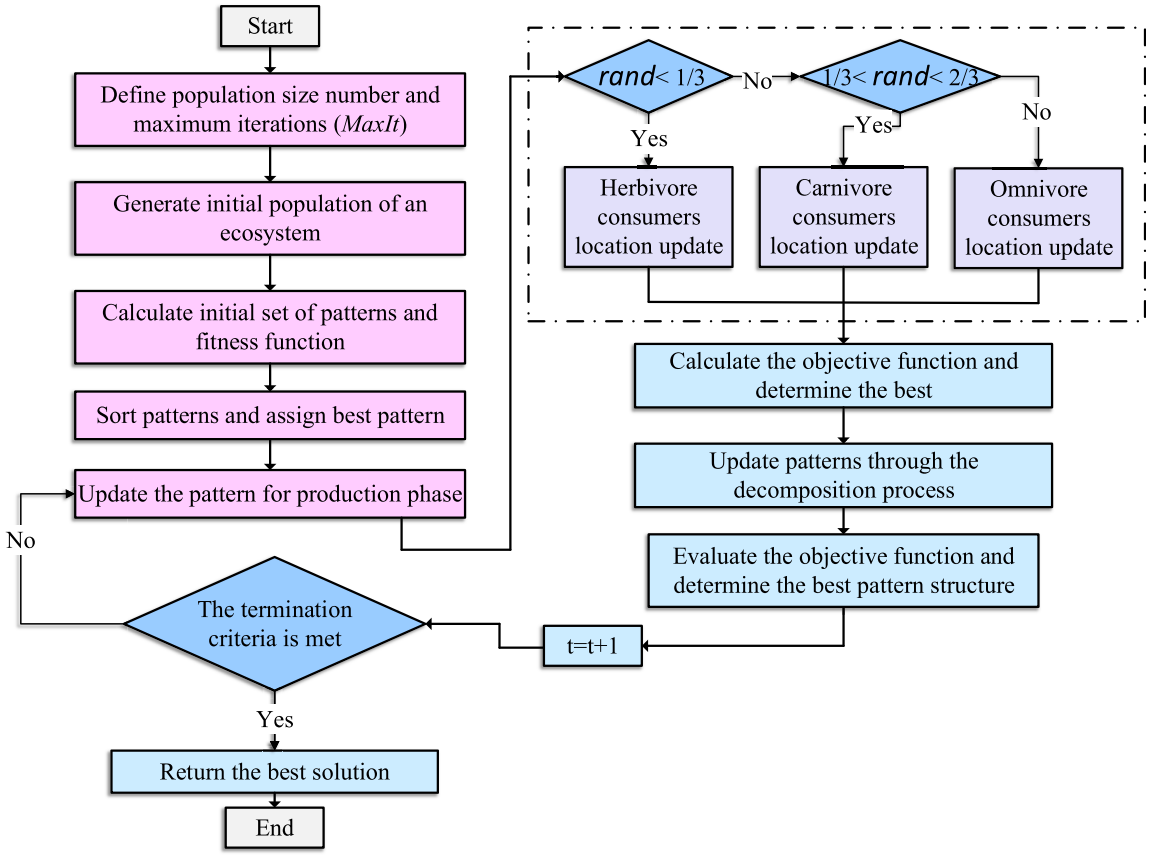

FIGURE 7. Flowchart of the AEO optimization method.

The driving objective function of the proposed optimized controllers design has to preserve minimized frequency deviations at area a (Δf_a) and at area b (Δf_b), in addition to mitigate the deviations of tie-line power (ΔP_{tie}). The ISE-based objective function of the proposed AEO-based optimized controllers design can be represented as follows:

$$ISE = \int_0^{t_s} \{(\Delta f_a)^2 + (\Delta f_b)^2 + (\Delta P_{tie})^2\} \tag{26}$$

Each of the utilized proposed controllers has 7 tuned parameters, which result in having total of 28 parameters that are tuned optimally using the proposed AEO method. The selected upper and lower boundaries that limit the selection ranges of each parameter can be represented as following:

$$\begin{aligned}
K_p^{min} &\le K_{p1}, K_{p2}, K_{p3}, K_{p4} \le K_p^{max} \\
K_t^{min} &\le K_{t1}, K_{t2}, K_{t3}, K_{t4} \le K_t^{max} \\
K_i^{min} &\le K_{i1}, K_{i2}, K_{i3}, K_{i4} \le K_i^{max} \\
K_d^{min} &\le K_{d1}, K_{d2}, K_{d3}, K_{d4} \le K_d^{max} \\
n^{min} &\le n_1, n_2, n_3, n_4 \le n^{max} \\
\lambda^{min} &\le \lambda_1, \lambda_2, \lambda_3, \lambda_4 \le \lambda^{max} \\
\mu^{min} &\le \mu_1, \mu_2, \mu_3, \mu_4, \le \mu^{max}
\end{aligned} \tag{27}$$

where, $(f)^{max}$ and $(f)^{min}$ represent the upper and lower limiting values, respectively for the controller parameters. The lower limits for the parameters (K_p^{min}, K_t^{min}, K_i^{min}, K_d^{min}) are set at zero, whereas the upper limits (K_p^{max}, K_t^{max}, K_i^{max}, K_d^{max}) are set at 20 in the proposed design method. The parameter n has lower limit n^{min} equals to 1 and upper limit n^{max} equals to 10. Whereas, the parameter μ has lower limit μ^{min} equals to 0 and upper limit μ^{max} equals to 1. The parameter λ has lower limit λ^{min} equals to 0 and upper limit λ^{max} equals to 1.

V. RESULTS AND DISCUSSIONS

Fig. 3 shows the case study of the interconnected multi-area power system. The overall system is modeled in SIMULINK/MATLAB environment to investigate its performance with different scenarios of RESs variations and load changes. The AEO algorithm is created by m-file and interfaced with the studied power system model to perform the optimization process. It has two main control parameters; maximum iterations = 100, and population size = 20. The convergence behavior of AEO method is investigated and compared with the other metaheuristic optimization techniques, such as genetic algorithm (GA), particle swarm optimization (PSO), and manta ray foraging optimization (MRFO) as shown in Fig. 8. The studied algorithms

TABLE 2. Optimized Controller Parameters for the Case Study.

Controller	Area	Control	Coefficients						
			K_t	K_p	K_i	K_d	λ	μ	n
Proposed	Area a	LFC	0.8262	1.9353	1.5308	1.216	0.45	0.27	2.72
		EV	1.0601	0.9534	1.2808	0.7357	0.31	0.19	3.11
	Area b	LFC	1.6419	1.7982	1.7110	1.9301	0.41	0.33	2.55
		EV	1.7164	1.9470	1.9867	0.3945	0.30	0.29	3.87
FOPID	Area a	LFC	-	1.6401	1.9148	1.3767	0.92	0.51	-
		EV	-	1.4049	1.4283	1.5170	0.94	0.72	-
	Area b	LFC	-	1.6372	1.8445	1.1588	0.89	0.57	-
		EV	-	0.2576	0.3992	0.8355	0.81	0.66	-
TID	Area a	LFC	1.4674	1.9704	1.8837	-	-	-	1.66
		EV	0.9578	0.4129	0.2180	-	-	-	2.05
	Area b	LFC	1.8878	1.9427	1.9834	-	-	-	2.14
		EV	0.0856	0.1210	0.4264	-	-	-	2.83
PID	Area a	LFC	-	1.3820	1.9950	1.2607	-	-	-
		EV	-	0.6173	1.5535	0.7196	-	-	-
	Area b	LFC	-	1.7944	1.8173	1.1092	-	-	-
		EV	-	0.0754	0.3057	0.9899	-	-	-

TABLE 3. Maximum Overshoot (MO), Maximum Undershoot (MU) and Settling Time (ST) for the Different Scenarios.

Scenario	Controller	Δf_a			Δf_b			ΔP_{tie}		
		MO	MU	ST	MO	MU	ST	MO	MU	ST
No. 1 (at 15s)	PID	0.0183	0.0516	69	0.0013	0.0322	78	0.0068	0.0311	45
	TID	0.0141	0.0452	61	0.0138	0.0374	56	0.0079	0.0321	47
	FOPID	0.0072	0.0376	52	0.0071	0.0348	54	0.0045	0.0282	55
	Proposed	—	0.0144	26	—	0.0079	28	—	0.0032	28
No. 2 (at 60s)	PID	0.0141	0.0551	99	0.0116	0.0458	95	0.0132	0.0483	95
	TID	0.0168	0.0638	95	0.0006	0.0364	107	0.0048	0.0514	90
	FOPID	0.0065	0.0544	85	0.0084	0.0353	99	0.0002	0.0431	88
	Proposed	—	0.0217	67	0.0002	0.0072	91	0.0007	0.0198	84
No. 4 (at 100s)	PID	0.0614	0.0199	112	0.0372	0.0025	131	0.0386	—	133
	TID	0.0592	0.0149	113	0.0352	0.0163	133	0.0477	0.0019	132
	FOPID	0.0509	0.0111	111	0.0328	0.0022	130	0.0485	0.0012	131
	Proposed	0.0137	—	106	0.0043	—	125	0.0031	—	111
No. 5 (at 100s)	PID	0.0579	0.0149	119	0.0407	0.0153	137	0.0441	—	129
	TID	0.0567	0.0137	117	0.0379	0.0097	138	0.0435	—	125
	FOPID	0.0478	0.0097	114	0.0344	0.0029	136	0.0359	—	121
	Proposed	0.0171	—	111	0.0066	0.0004	128	0.0044	0.0002	113
No. 6 (at 85s)	PID	0.1584	0.1789	Osc.	0.1393	0.1014	Osc.	0.1316	0.0911	Osc.
	TID	0.0793	0.0542	99	0.0626	0.0226	105	0.0611	0.0261	103
	FOPID	0.0775	0.0354	95	0.0539	0.0085	100	0.0492	0.0191	99
	Proposed	0.0143	—	89	0.0056	—	94	0.0022	—	100
No. 7 (at 15s)	PID	0.4209	0.4319	Osc.	0.4185	0.4258	Osc.	0.4224	0.4235	Osc.
	TID	0.1835	0.1851	Osc.	0.1132	0.1147	Osc.	0.1473	0.1467	Osc.
	FOPID	0.1228	0.1245	Osc.	0.0989	0.1006	Osc.	0.0938	0.0934	Osc.
	Proposed	0.0078	0.0649	65	0.0169	0.0247	87	0.0023	0.0096	83

* ST denotes to settle time in seconds
** Osc. denotes to undamped oscillation condition

are tested at step load, multiple load steps and random load cases. It can be seen that the AEO method possesses a more smooth curve with faster convergence rate than the other studied algorithms for the three studied cases. The MRFO method comes in the second order after the AEO, while the GA and PSO suffer from premature convergence caused by the particles stagnating around local optima. All the controller parameters are computed using the AEO optimization algorithm as shown in Table 2. Under the same operating conditions, several scenarios have been conducted to compare the dynamic performance of the the proposed controller with respect to the conventional PID, FOPID and TID controllers in order to explore the superiority of the proposed controller.

Throughout the simulation results, it is assumed that all EVs have the same capacities in the two-area, where it represents 10% penetration levels of the power system base. The initial SOC of EV_a and EV_b is assumed as 95%. The simulation results are carried out with considering the thermal unit with generation constraint (GRC) of 10%/min and hydro unit with 270%/min up and 360%/min down generation [37]. The proposed AEO-based controller is tested under different disturbances of step, multiple and random load profiles. The effectiveness and robustness of the proposed controller have been investigated with such sever conditions such as high fluctuations in the RESs and different penetration levels of EVs.

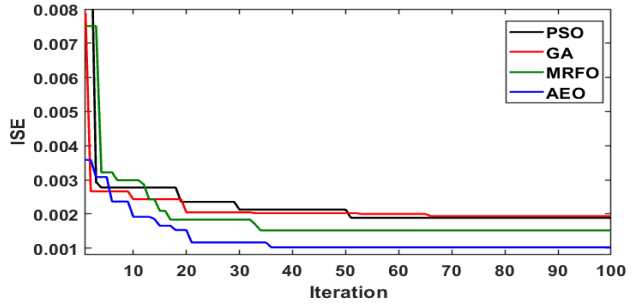

(a) Step load case

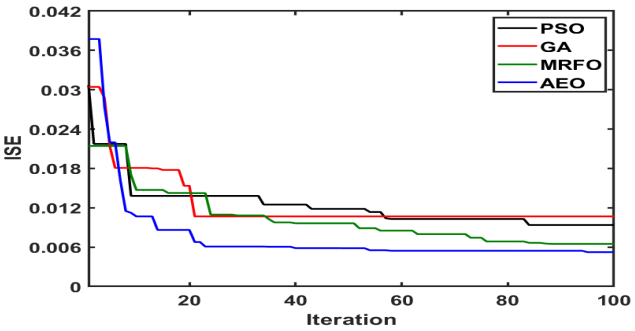

(b) Multiple load steps case

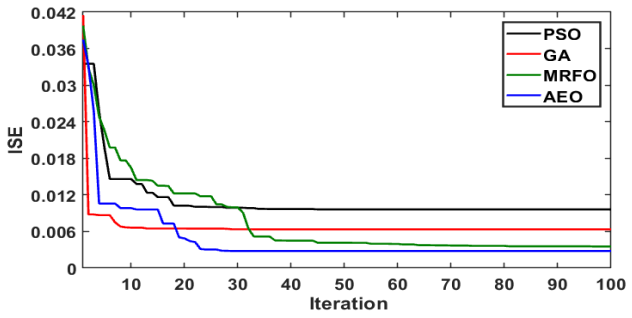

(c) Random load case

FIGURE 8. Comparison of the conversion curves of the AEO method and other metaheuristic optimization techniques.

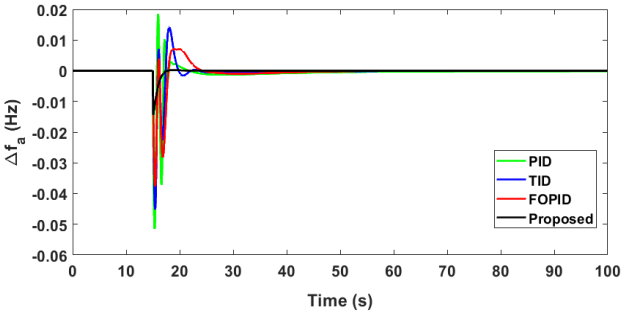

(a) Δf_a

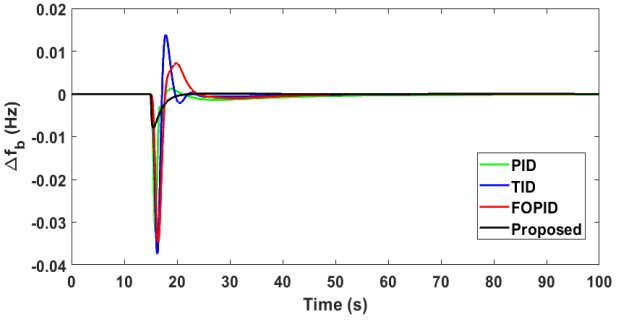

(b) Δf_b

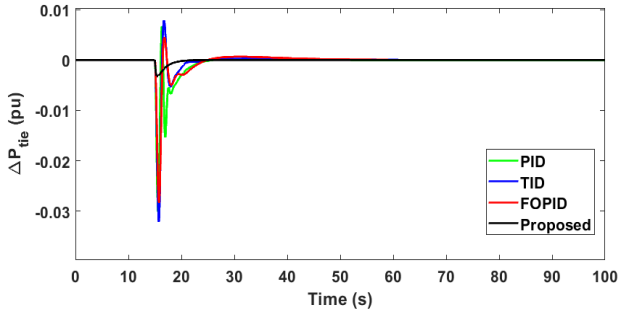

(c) ΔP_{tie}

FIGURE 9. System dynamic response for scenario 1.

A. SCENARIO 1: LOAD STEP CHANGE

In this scenario, system performance with the developed controllers is investigated against 10% step load change at time 15s in area *a* without RESs. Fig. 9a and Fig. 9b show the frequency deviation waveforms in area *a* and *b*, respectively. Using the proposed optimized controller for LFC and EVs, it can be noted that the system frequency deviations have the minimum over/under shoots and settling time compared to the other conventional controllers. The response shows that the proposed controllers are successful at damping out the frequency oscillations with minimized overshoot/undershoot values. Table 3 summarizes the obtained results of maximum overshoot/undershoot values in addition to settling time for the studied scenarios. The proposed controller has undershoot value of 0.0144 in area *a* compared to 0.0516, 0.0452, and 0.0376 for the PID, TID, and FOPID controllers, respectively. The same observations are clear in the obtained results. In addition, the proposed controller has the lowest oscillations magnitude and duration of the tie-line power in comparison with conventional controllers as depicted in Fig. 9c. Fig. 10a and Fig. 10b show the response of SOC of EVs in area *a* and area *b*, respectively. Moreover, it has become clear that the proposed method enables the proper cooperation between the LFC and EV. This in turn is reflected as faster discharge process at classical controllers compared to the proposed controller. Complying to the ACE fundamentals, the tie-line power between the two areas *a* and *b* is vanished in the steady state, which means that area *a* provides the sufficient generations from its local sources to cover this step load change. The thermal power plant and the electrical vehicles in area *a* share together the required generation to restore the frequency deviation in area *a* to its original value.

B. SCENARIO 2: MULTIPLE LOAD CHANGE

In this scenario, a multiple load stepping profile with three perturbation steps is applied to the studied power system at

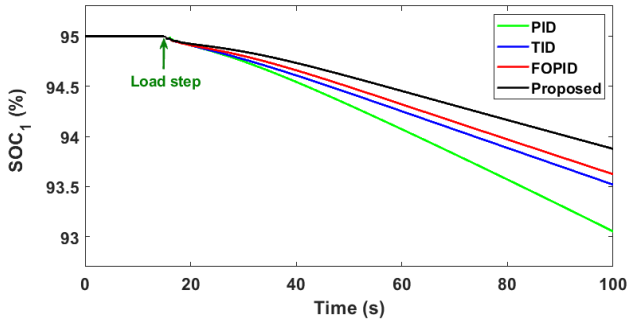

(a) SOC_1 (%) at scenario 1

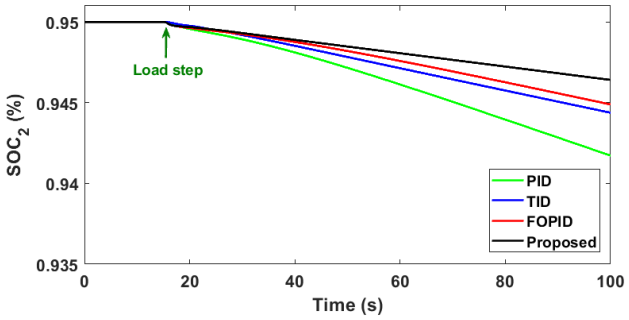

(b) SOC_2 (%) at scenario 1

FIGURE 10. SOC response for scenario 1.

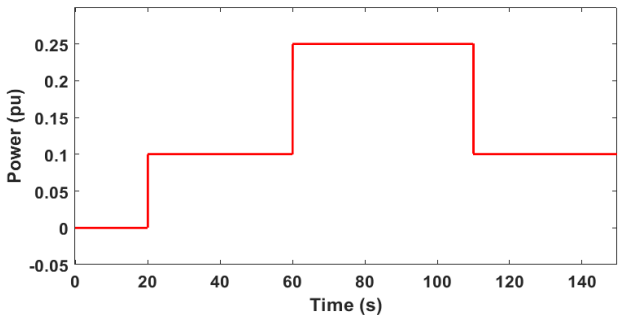

FIGURE 11. Load profile for scenario 2.

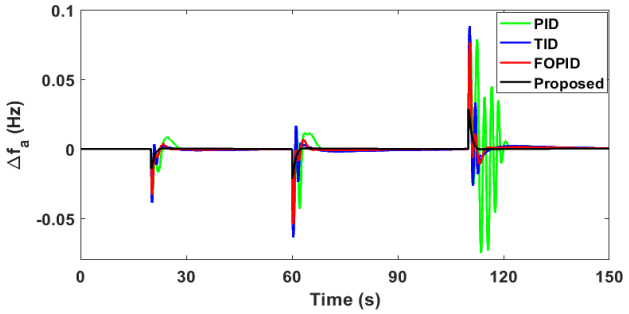

(a) Δf_a

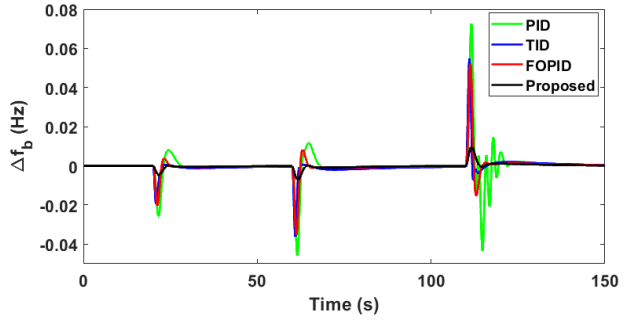

(b) Δf_b

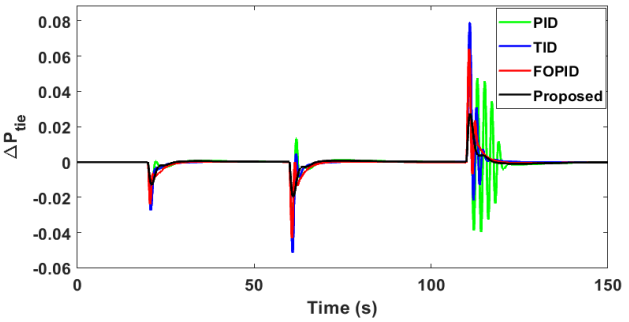

(c) ΔP_{tie}

FIGURE 12. System dynamic response for scenario 2.

20s, 60s, 110s as shown in Fig. 11. The simulation results of the dynamic response of system frequency and tie-line power deviations are shown in Fig. 12. It is obvious from the results that the proposed controller guarantees system stability with the lowest overshoot, as the proposed controller decreases the overshoot in the frequency deviation more than 50% compared to the other conventional controllers. The calculations for this scenario for the maximum overshoot/undershoot and the settling time values are added to Table 3. Moreover, the proposed controllers are successful at maintaining the slow charge of the EVs in both areas compared to the deep discharge process under the other conventional controllers as shown in Fig. 13a and Fig. 13b. Further, the controller succeeded to restore the tie-line power between the two areas to its original value, and the step load changes have been balanced by the increased generations for the area *a* sources.

C. SCENARIO 3: RANDOM LOAD CHANGE

To demonstrate the performance and efficiency of the proposed controller, the performance of the two-area power system is examined while considering a random load variation instead of the multiple load stepping profile in the previous scenario. Fig. 14 shows the load power of the considered random load profile. The obtained frequency and tie-line power results are depicted in Fig. 15. It can be seen that the PID, TID, and FOPID control systems have poor damping characteristic for the deviations in the system frequency and tie-line power during the load fluctuations. However, the proposed controller indicates significantly improved performance at minimizing the overshoot values and settling time of frequency and tie-line power deviations during the overall load change in comparison with PID, FOPID, and TID controllers. Furthermore, the proposed controller for the EVs system achieves better performance as it succeeded in managing the SOC of the EVs in both

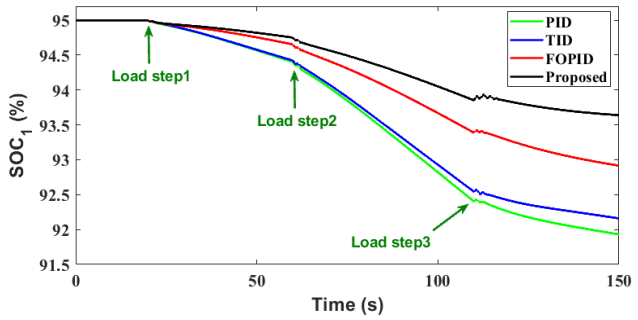

(a) SOC_1 (%) at scenario 2

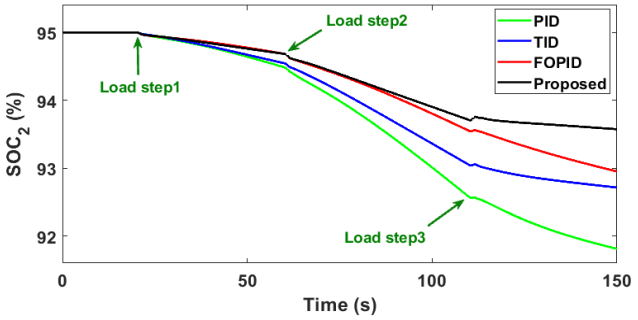

(b) SOC_2 (%) at scenario 2

FIGURE 13. SOC response for scenario 2.

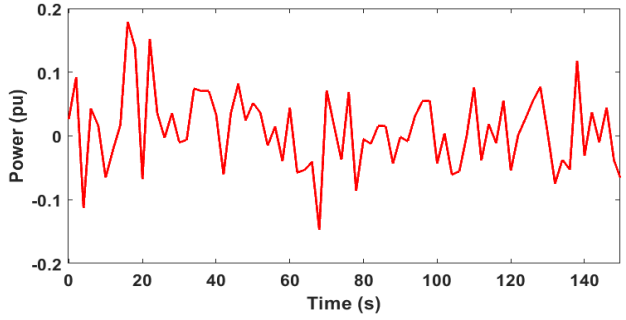

FIGURE 14. Generation profile for scenario 3.

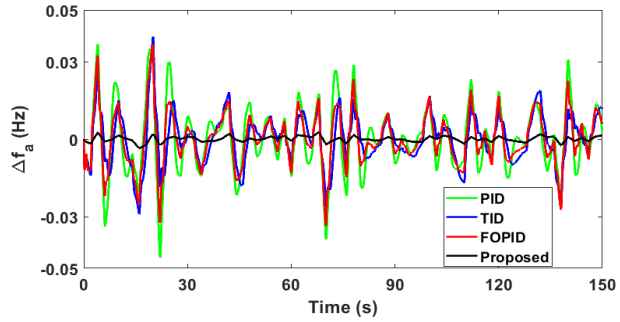

(a) Δf_a

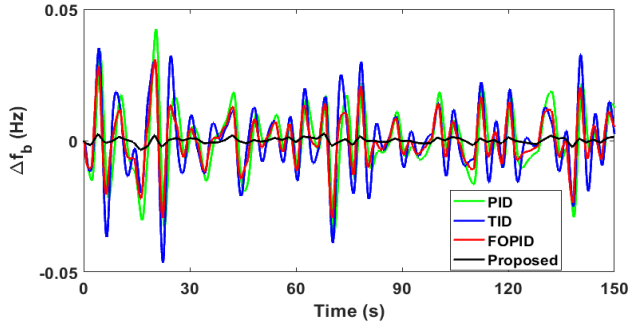

(b) Δf_b

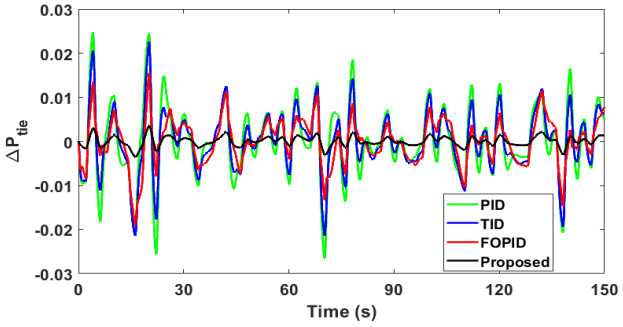

(c) ΔP_{tie}

FIGURE 15. System dynamic response for scenario 3.

areas *a* and *b* in an efficient manner. This is due that the proposed controllers achieves the cooperative share between the LFC and EV controllers. Thence, they respond to the multi-area system frequency faster than the other controllers as seen in Fig. 16a, and Fig. 16b for SOC_1 and SOC_2, respectively.

D. SCENARIO 4: IMPACT OF RESs

In this scenario, an extreme case of high fluctuated wind generation, which is connected at 100s beside a 10% step load change at 15s, is applied to area *a* to evaluate the robustness of the proposed modified controller. The load power and wind profile of this scenario are shown in Fig. 17. The performance of frequency deviations and the tie-line power are shown in Fig. 18. As shown in Table 3, the proposed controller confirms high capability to suppress system transient oscillations compared to the conventional controllers. The system oscillations have been damped out within 25s with the proposed controller against 39s, 57s, 65s for FOPID, TID, and PID, respectively. Moreover, as shown in Fig. 19a and Fig. 19b, the proposed controller has a significant impact on SOC of the EVs. It shows that the discharging rate of the EVs in both areas using the proposed controller is lower than the other controllers. This in turn means that the proposed controller has a very fast action to suppress frequency deviation and the tie-line power fluctuation. Moreover, proper coordination among the LFC and EV controllers is achieved using the proposed modified controller.

E. SCENARIO 5: UNCERTAINTY ANALYSIS

In this tested scenario, the power system is examined under the same circumstances of the above scenario with varying system parameters by 35% reduction. Fig. 20a, and Fig. 20b show the frequency deviations in both areas with

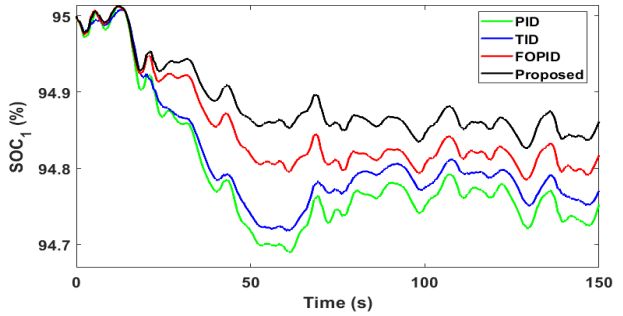

(a) SOC_1 (%) at scenario 3

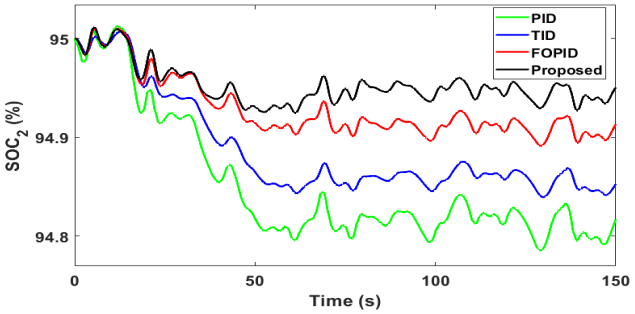

(b) SOC_2 (%) at scenario 3

FIGURE 16. SOC response for scenario 3.

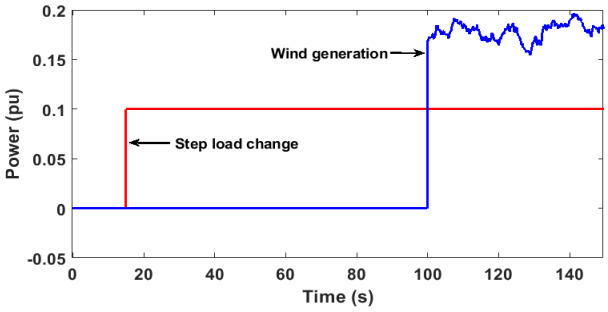

FIGURE 17. Generation profile for scenario 4.

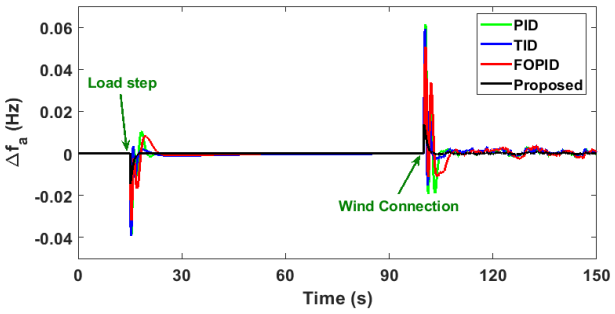

(a) Δf_a

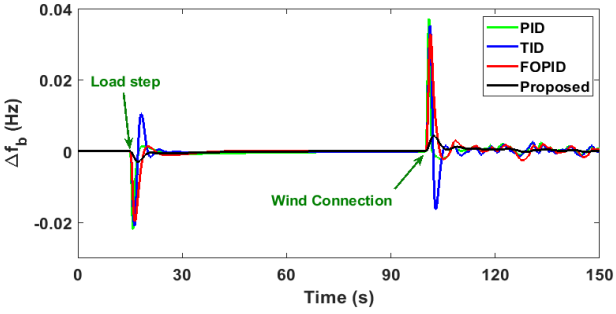

(b) Δf_b

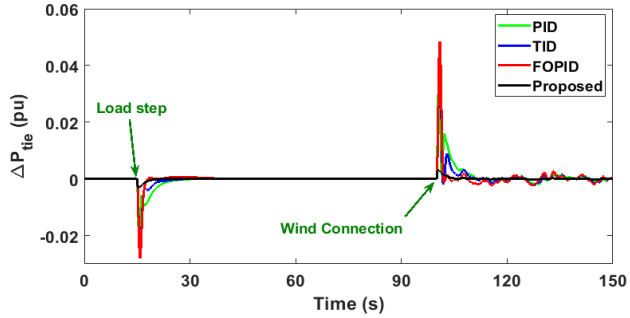

(c) $\Delta P_{tie,eq}$

FIGURE 18. System dynamic response for scenario 4.

PID, FOPID, and TID controllers compared with previous scenario. However, the proposed controller still has a satisfactory response in damping these deviations to an acceptable level. Furthermore, it can damp the transient tie-line power oscillations very quickly with settling time of 22s compared to 37s, 43s, 66s for FOPID, TID, and PID, respectively as depicted in Fig. 20c. Moreover, the effectiveness of the new controller has become clear in the response of the EVs charge/discharge operation in the two areas. Fig. 21a, and Fig. 21b proves that the proposed controller has better performance in handling the SOC of EVs than the other control methods. It can be discharged at step load change at 15s and charged with wind insertion at time of 100s in quick action and with lowest power sharing compared to the conventional controllers. Hence, it is evident from Fig. 20, Fig. 21a, Fig. 21b and Table 3 that the new proposed modified controller improves the whole dynamic system stability in terms of frequency and power overshoot, undershoot, and settling time.

F. SCENARIO 6: HIGH PENETRATION OF RESs

To perform more severe scenario, the two-area power system is studied after adding a PV generation power source with multiple stepping load variations, and high wind power fluctuations as shown in Fig. 22. It is seen in Fig. 23a, and Fig. 23b that the PID controller is capable of controlling and restoring the frequency to the steady-state value under the load disturbances of 20s and 50s, respectively. While it cannot withstand the large change of system frequency caused by integrating high wind generation at 85s, where system frequency fluctuations in this case reaches high values leading to system instability. Moreover, the TID and the FOPID control systems provide satisfactory results in comparison with the PID controller with reasonable capability

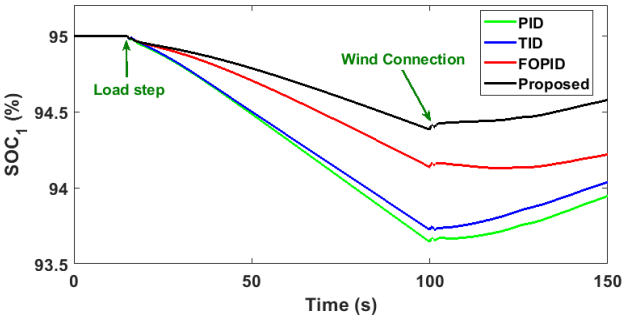

(a) SOC_1 (%) at scenario 4

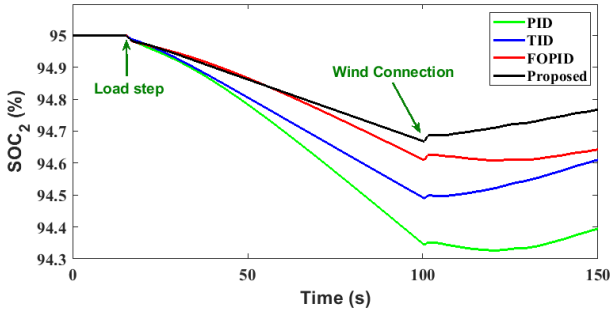

(b) SOC_2 (%) at scenario 4

FIGURE 19. SOC response for scenario 4.

TABLE 4. Performance Indices for the Selected Cases Study.

Scenario	Controller	Performance indices		
		ISE	ITSE	IAE
No.1	PID	0.029	0.0448	0.2103
	TID	0.021	0.0378	0.1527
	FOPID	0.018	0.0312	0.1427
	Proposed	0.0014	0.0101	0.1252
No.2	PID	0.0258	1.4354	0.6164
	TID	0.0181	1.1395	0.6187
	FOPID	0.0128	0.7852	0.5361
	Proposed	0.0058	0.1928	0.2232
No.3	PID	0.0568	2.8955	3.8353
	TID	0.0498	2.2089	3.2115
	FOPID	0.0279	1.6780	2.3926
	Proposed	0.0032	1.0512	1.2142
No.4	PID	0.0249	0.5903	0.4598
	TID	0.0151	0.4009	0.3699
	FOPID	0.0142	0.3319	0.3552
	Proposed	0.0028	0.1888	0.1788
No.5	PID	0.0943	0.4417	0.4607
	TID	0.0343	0.3366	0.3515
	FOPID	0.0238	0.2978	0.3524
	Proposed	0.0025	0.0505	0.0875
No.6	PID	0.0452	3.9099	1.9480
	TID	0.0398	3.0732	1.3908
	FOPID	0.0360	2.7430	1.1092
	Proposed	0.0086	1.0129	0.3466
No.7	PID	3.0067	260.71	75.953
	TID	2.3072	196.12	28.323
	FOPID	1.7013	143.08	21.366
	Proposed	0.0047	0.0898	0.3839

at damping out the frequency oscillations in addition to the tie-line power deviations as seen in Fig. 23. In contrast,

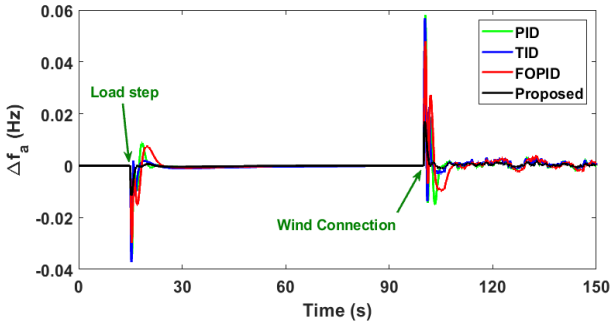

(a) Δf_a

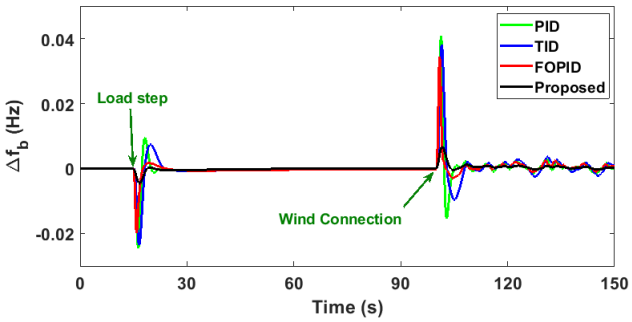

(b) Δf_b

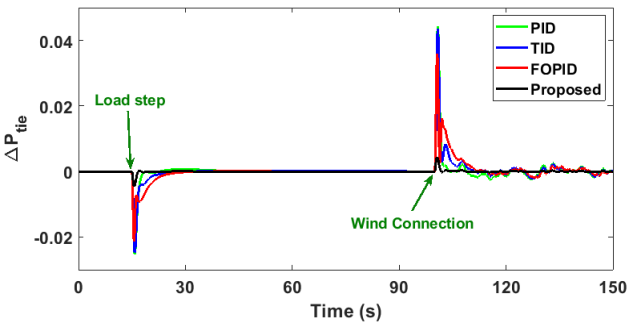

(c) ΔP_{tie}

FIGURE 20. System dynamic response for scenario 5.

the proposed modified controller based on the AEO algorithm offers superior performance by effectively handling this contingency. Therefore, this severe case represents a powerful proof for the effectiveness and robustness of the new proposed controller over other existing comparative methods.

G. SCENARIO 7: IMPACT OF EV

In this scenario, the effect of EVs capacity on the dynamic performance of the multi-area system is studied. This case is examined on the same conditions of scenario 1 with step load change of 10% and 50% reduction of the number of connected EVs. Fig. 24 shows the deviations of frequency and tie-line power of the studied system. It is obvious from the obtained results that the PID, FOPID, and TID controllers are very sensitive to the change of EVs capacity as they suffer from prolonged oscillations and hence they cannot restore the power system frequency in addition to

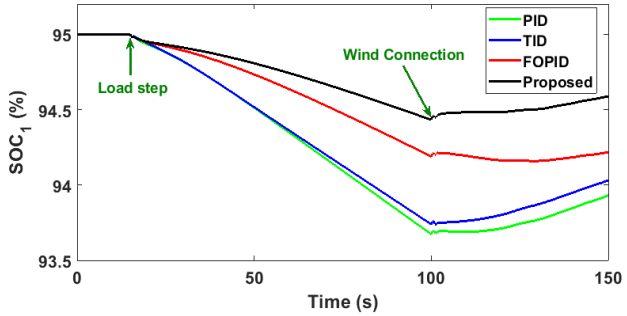

(a) SOC_1 (%) at scenario 5

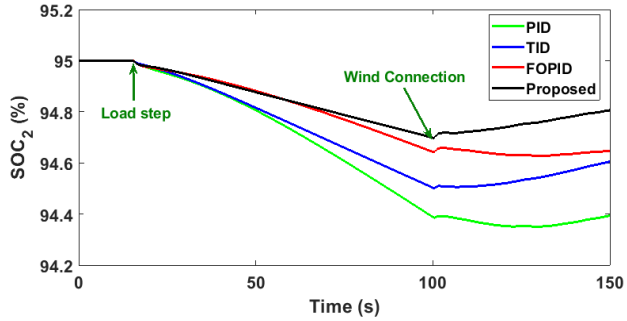

(b) SOC_2 (%) at scenario 5

FIGURE 21. SOC response for scenario 5.

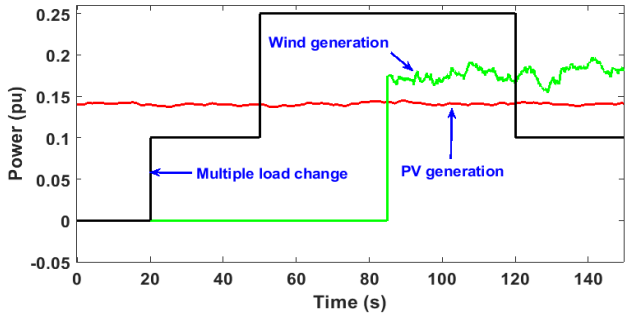

FIGURE 22. Generation profile for scenario 6.

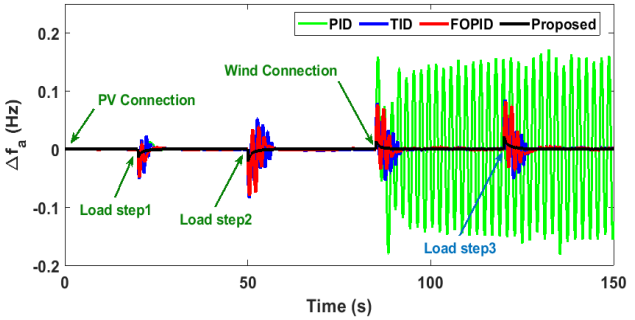

(a) Δf_a

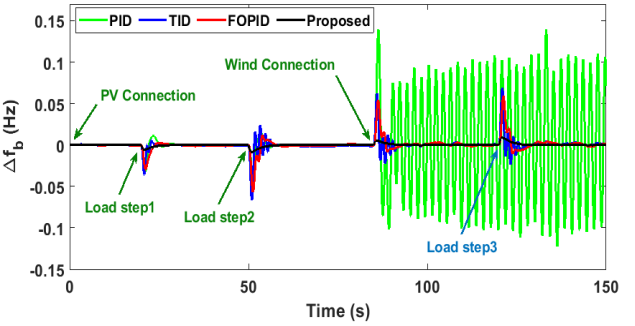

(b) Δf_b

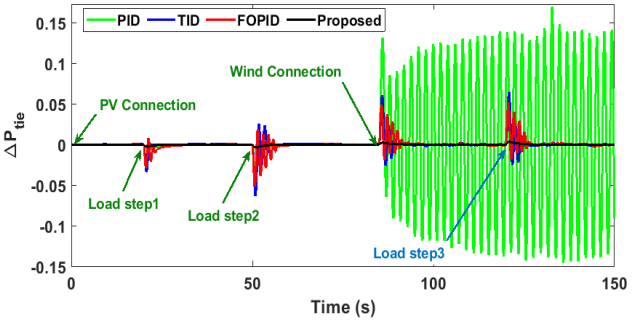

(c) ΔP_{tie}

FIGURE 23. System dynamic response for scenario 6.

the tie-line power at their original values at reduced number of connected EVs. Therefore, the percentage share of EVs capacity has a great effect on enhancing the frequency regulation of the multi-area system and its response with conventional controllers. On the other hand, the proposed controller succeeds in treating this contingency regardless of the decreased number of EVs as shown in the obtained results of Fig. 24. Hence, the outcome of this case assures the efficiency of the proposed hybrid controller on the LFC and EVs systems.

H. PERFORMANCE COMPARISON

Different types of the performance indices have been calculated using the addressed controllers and tabulated in Table 4. The comparison includes the ISE in addition to the widely-used indices of the integral-absolute error (IAE) and the integral time-squared error (ITSE) [54]. The proposed controller achieves better values for the performance indices ISE, ITSE and IAE than the other conventional ones. The estimated indices show the superiority of the proposed controllers over the classical ones. For instance, at scenario 1, the ISE values are 0.029, 0.021, and 0.018 for the PID, TID, and FOPID controllers, respectively in comparison with 0.0014 under the proposed method. It can be observed that the ISE value of the proposed method is 4.83%, 6.67%, and 7.78% of the ISE values under the PID, TID, and FOPID controllers, respectively. Whereas, the ITSE values are 0.0448, 0.0378, 0.0312, and 0.0101 for the PID, TID, FOPID and the proposed controller, respectively. The ITSE values for the proposed method are 22.54%, 26.72%, and 32.37% of the ITSE values with PID, TID, and FOPID controllers, respectively. The same improvements can be observed with the other criteria and the whole studied scenarios.

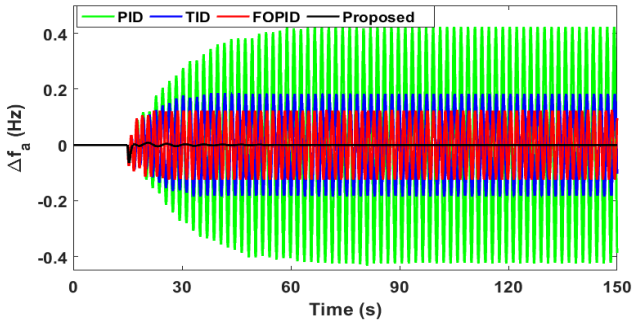

(a) Δf_a

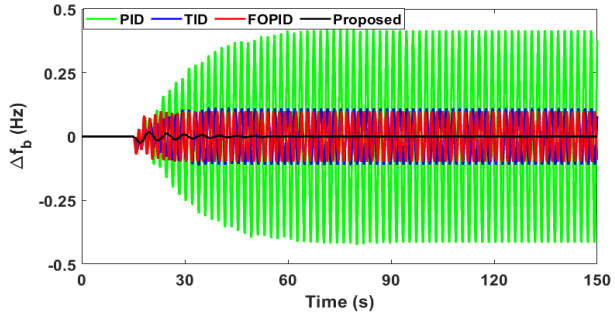

(b) Δf_b

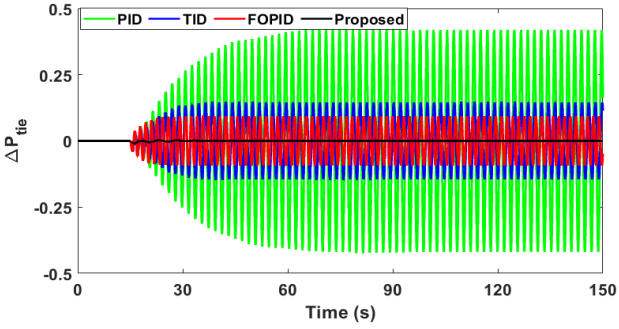

(c) ΔP_{tie}

FIGURE 24. System dynamic response for scenario 7.

VI. CONCLUSION

This article proposes an optimized modified fractional order cooperative controller for LFC and EVs in multi-area power system. The proposed controller merges the benefits of both the FOPID and the TID control systems. Moreover, an employment of a recent artificial ecosystem optimization (AEO) algorithm for determining the secondary controller's parameters is also developed. The simulation results show the effectiveness of the developed controllers compared to the used conventional controllers (PID, TID, FOPID) particularly with the fluctuated nature of the RESs and the decreased penetration levels of the EVs. The proposed LFC and EV controllers have the capability of damping out the frequency oscillations and to regulate the tie-line power, where minimized overshoot/undershoot values and settling time have been achieved. In addition, the simulation results show the capability of the proposed cooperative controller to suppress system fluctuations and retain system stability with reduced number of EVs compared to the other conventional controllers. This in turn becomes advantageous through decreasing EVs loading and enhancing their lifetime.

REFERENCES

[1] S. M. Said, M. Aly, B. Hartmann, A. G. Alharbi, and E. M. Ahmed, "SMES-based fuzzy logic approach for enhancing the reliability of microgrids equipped with PV generators," *IEEE Access*, vol. 7, pp. 92059–92069, 2019.

[2] E. M. Ahmed, M. Aly, A. Elmelegi, A. G. Alharbi, and Z. M. Ali, "Multifunctional distributed MPPT controller for 3P4W grid-connected PV systems in distribution network with unbalanced loads," *Energies*, vol. 12, no. 24, p. 4799, Dec. 2019.

[3] E. A. Mohamed and Y. Mitani, "Load frequency control enhancement of islanded micro-grid considering high wind power penetration using superconducting magnetic energy storage and optimal controller," *Wind Eng.*, vol. 43, no. 6, pp. 609–624, Jan. 2019.

[4] S. M. Said, M. Aly, and H. Balint, "An efficient reactive power dispatch method for hybrid photovoltaic and superconducting magnetic energy storage inverters in utility grids," *IEEE Access*, vol. 8, pp. 183708–183721, 2020.

[5] C. Rahmann, S. I. Chamas, R. Alvarez, H. Chavez, D. Ortiz-Villalba, and Y. Shklyarskiy, "Methodological approach for defining frequency related grid requirements in low-carbon power systems," *IEEE Access*, vol. 8, pp. 161929–161942, 2020.

[6] G. Perkins, "Techno-economic comparison of the levelised cost of electricity generation from solar PV and battery storage with solar PV and combustion of bio-crude using fast pyrolysis of biomass," *Energy Convers. Manage.*, vol. 171, pp. 1573–1588, Sep. 2018.

[7] E. Mohamed, A.-A.-A. Mohamed, and Y. Mitani, "Genetic-moth swarm algorithm for optimal placement and capacity of renewable DG sources in distribution systems," *Int. J. Interact. Multimedia Artif. Intell.*, vol. 5, no. 7, p. 105, 2019, doi: 10.9781/ijimai.2019.10.005.

[8] E. A. Mohamed and Y. Mitani, "Enhancement the dynamic performance of islanded microgrid using a coordination of frequency control and digital protection," *Int. J. Emerg. Electr. Power Syst.*, vol. 20, no. 1, Feb. 2019, Art. no. 20180136.

[9] S. Saxena, "Load frequency control strategy via fractional-order controller and reduced-order modeling," *Int. J. Electr. Power Energy Syst.*, vol. 104, pp. 603–614, Jan. 2019.

[10] S. Prasad, S. Purwar, and N. Kishor, "Load frequency regulation using observer based non-linear sliding mode control," *Int. J. Electr. Power Energy Syst.*, vol. 104, pp. 178–193, Jan. 2019.

[11] M. Khan, H. Sun, Y. Xiang, and D. Shi, "Electric vehicles participation in load frequency control based on mixed H_2/H_∞," *Int. J. Electr. Power Energy Syst.*, vol. 125, Feb. 2021, Art. no. 106420.

[12] M. Z. Bernard, T. H. Mohamed, Y. S. Qudaih, and Y. Mitani, "Decentralized load frequency control in an interconnected power system using coefficient diagram method," *Int. J. Electr. Power Energy Syst.*, vol. 63, pp. 165–172, Dec. 2014.

[13] N. B. Arias, S. Hashemi, P. B. Andersen, C. Træholt, and R. Romero, "Assessment of economic benefits for EV owners participating in the primary frequency regulation markets," *Int. J. Electr. Power Energy Syst.*, vol. 120, Sep. 2020, Art. no. 105985.

[14] H. Jia, X. Li, Y. Mu, C. Xu, Y. Jiang, X. Yu, J. Wu, and C. Dong, "Coordinated control for EV aggregators and power plants in frequency regulation considering time-varying delays," *Appl. Energy*, vol. 210, pp. 1363–1376, Jan. 2018.

[15] M. Dreidy, H. Mokhlis, and S. Mekhilef, "Inertia response and frequency control techniques for renewable energy sources: A review," *Renew. Sustain. Energy Rev.*, vol. 69, pp. 144–155, Mar. 2017.

[16] S. K. Pandey, S. R. Mohanty, and N. Kishor, "A literature survey on load–frequency control for conventional and distribution generation power systems," *Renew. Sustain. Energy Rev.*, vol. 25, pp. 318–334, Sep. 2013.

[17] R. Shankar, S. R. Pradhan, K. Chatterjee, and R. Mandal, "A comprehensive state of the art literature survey on LFC mechanism for power system," *Renew. Sustain. Energy Rev.*, vol. 76, pp. 1185–1207, Sep. 2017.

[18] A. Khalil, Z. Rajab, A. Alfergani, and O. Mohamed, "The impact of the time delay on the load frequency control system in microgrid with plug-in-electric vehicles," *Sustain. Cities Soc.*, vol. 35, pp. 365–377, Nov. 2017.

[19] M. S. Ayas and E. Sahin, "FOPID controller with fractional filter for an automatic voltage regulator," *Comput. Electr. Eng.*, early access, Nov. 2020, Art. no. 106895.

[20] J. Sharma, Y. V. Hote, and R. Prasad, "PID controller design for interval load frequency control system with communication time delay," *Control Eng. Pract.*, vol. 89, pp. 154–168, Aug. 2019.

[21] D. Yousri, T. S. Babu, and A. Fathy, "Recent methodology based Harris Hawks optimizer for designing load frequency control incorporated in multi-interconnected renewable energy plants," *Sustain. Energy, Grids Netw.*, vol. 22, Jun. 2020, Art. no. 100352.

[22] A. Oshnoei, R. Khezri, S. M. Muyeen, S. Oshnoei, and F. Blaabjerg, "Automatic generation control incorporating electric vehicles," *Electr. Power Compon. Syst.*, vol. 47, no. 8, pp. 720–732, May 2019.

[23] N. Hakimuddin, I. Nasiruddin, T. S. Bhatti, and Y. Arya, "Optimal automatic generation control with hydro, thermal, gas, and wind power plants in 2-Area interconnected power system," *Electr. Power Compon. Syst.*, vol. 48, nos. 6–7, pp. 558–571, Apr. 2020.

[24] G. Magdy, A. Bakeer, M. Nour, and E. Petlenkov, "A new virtual synchronous generator design based on the SMES system for frequency stability of low-inertia power grids," *Energies*, vol. 13, no. 21, p. 5641, Oct. 2020.

[25] Y. Arya, "Impact of ultra-capacitor on automatic generation control of electric energy systems using an optimal FFOID controller," *Int. J. Energy Res.*, vol. 43, no. 14, pp. 8765–8778, Aug. 2019, doi: 10.1002/er.4767.

[26] S. Priyadarshani, K. R. Subhashini, and J. K. Satapathy, "Pathfinder algorithm optimized fractional order tilt-integral-derivative (FOTID) controller for automatic generation control of multi-source power system," *Microsyst. Technol.*, vol. 27, no. 1, pp. 23–35, Jun. 2020.

[27] Y. Arya, "A novel CFFOPI-FOPID controller for AGC performance enhancement of single and multi-area electric power systems," *ISA Trans.*, vol. 100, pp. 126–135, May 2020.

[28] P. Jampeethong and S. Khomfoi, "Coordinated control of electric vehicles and renewable energy sources for frequency regulation in microgrids," *IEEE Access*, vol. 8, pp. 141967–141976, 2020.

[29] Y. Arya, "Effect of electric vehicles on load frequency control in interconnected thermal and hydrothermal power systems utilising CF-FOIDF controller," *IET Gener., Transmiss. Distrib.*, vol. 14, no. 14, pp. 2666–2675, Jul. 2020.

[30] Y. Arya, P. Dahiya, E. Çelik, G. Sharma, H. Gözde, and I. Nasiruddin, "AGC performance amelioration in multi-area interconnected thermal and thermal-hydro-gas power systems using a novel controller," *Eng. Sci. Technol., Int. J.*, pp. 1–13, Oct. 2020.

[31] Y. A. Dahab, H. Abubakr, and T. H. Mohamed, "Adaptive load frequency control of power systems using electro-search optimization supported by the balloon effect," *IEEE Access*, vol. 8, pp. 7408–7422, 2020.

[32] A. Daraz, S. A. Malik, H. Mokhlis, I. U. Haq, F. Zafar, and N. N. Mansor, "Improved-fitness dependent optimizer based FOI-PD controller for automatic generation control of multi-source interconnected power system in deregulated environment," *IEEE Access*, vol. 8, pp. 197757–197775, 2020.

[33] Y. Arya, "Impact of hydrogen Aqua electrolyzer-fuel cell units on automatic generation control of power systems with a new optimal fuzzy TIDF-II controller," *Renew. Energy*, vol. 139, pp. 468–482, Aug. 2019.

[34] R. K. Sahu, S. Panda, A. Biswal, and G. T. C. Sekhar, "Design and analysis of tilt integral derivative controller with filter for load frequency control of multi-area interconnected power systems," *ISA Trans.*, vol. 61, pp. 251–264, Mar. 2016.

[35] S. Malik and S. Suhag, "A novel SSA tuned PI-TDF control scheme for mitigation of frequency excursions in hybrid power system," *Smart Sci.*, vol. 8, no. 4, pp. 202–218, Sep. 2020.

[36] A. Latif, S. M. S. Hussain, D. C. Das, and T. S. Ustun, "Optimum synthesis of a BOA optimized novel dual-stage PI-(1 + ID) controller for frequency response of a microgrid," *Energies*, vol. 13, no. 13, p. 3446, Jul. 2020.

[37] E. A. Mohamed, E. M. Ahmed, A. Elmelegi, M. Aly, O. Elbaksawi, and A.-A.-A. Mohamed, "An optimized hybrid fractional order controller for frequency regulation in multi-area power systems," *IEEE Access*, vol. 8, pp. 213899–213915, 2020.

[38] Y. Arya, N. Kumar, P. Dahiya, G. Sharma, E. Çelik, S. Dhundhara, and M. Sharma, "Cascade-I^{λ} D^{μ} N controller design for AGC of thermal and hydro-thermal power systems integrated with renewable energy sources," *IET Renew. Power Gener.*, early access, pp. 1–17, Jan. 2021, doi: 10.1049/rpg2.12061.

[39] H. H. Ali, A. Fathy, and A. M. Kassem, "Optimal model predictive control for LFC of multi-interconnected plants comprising renewable energy sources based on recent sooty terns approach," *Sustain. Energy Technol. Assessments*, vol. 42, Dec. 2020, Art. no. 100844.

[40] H. H. Ali, A. M. Kassem, M. Al-Dhaifallah, and A. Fathy, "Multi-verse optimizer for model predictive load frequency control of hybrid multi-interconnected plants comprising renewable energy," *IEEE Access*, vol. 8, pp. 114623–114642, 2020.

[41] A. Bagheri, A. Jabbari, and S. Mobayen, "An intelligent ABC-based terminal sliding mode controller for load-frequency control of islanded micro-grids," *Sustain. Cities Soc.*, vol. 64, Jan. 2021, Art. no. 102544.

[42] J. Guo, "Application of full order sliding mode control based on different areas power system with load frequency control," *ISA Trans.*, vol. 92, pp. 23–34, Sep. 2019.

[43] S. Falahati, S. A. Taher, and M. Shahidehpour, "Grid secondary frequency control by optimized fuzzy control of electric vehicles," *IEEE Trans. Smart Grid*, vol. 9, no. 6, pp. 5613–5621, Nov. 2018.

[44] M. U. Jan, A. Xin, M. A. Abdelbaky, H. U. Rehman, and S. Iqbal, "Adaptive and fuzzy PI controllers design for frequency regulation of isolated microgrid integrated with electric vehicles," *IEEE Access*, vol. 8, pp. 87621–87632, 2020.

[45] N. Jalali, H. Razmi, and H. Doagou-Mojarrad, "Optimized fuzzy self-tuning PID controller design based on tribe-DE optimization algorithm and rule weight adjustment method for load frequency control of interconnected multi-area power systems," *Appl. Soft Comput.*, vol. 93, Aug. 2020, Art. no. 106424.

[46] X. Luo, S. Xia, and K. W. Chan, "A decentralized charging control strategy for plug-in electric vehicles to mitigate wind farm intermittency and enhance frequency regulation," *J. Power Sources*, vol. 248, pp. 604–614, Feb. 2014.

[47] Y. Ota, H. Taniguchi, T. Nakajima, K. M. Liyanage, J. Baba, and A. Yokoyama, "Autonomous distributed V2G (vehicle-to-grid) satisfying scheduled charging," *IEEE Trans. Smart Grid*, vol. 3, no. 1, pp. 559–564, Mar. 2012.

[48] S. Falahati, S. A. Taher, and M. Shahidehpour, "A new smart charging method for EVs for frequency control of smart grid," *Int. J. Electr. Power Energy Syst.*, vol. 83, pp. 458–469, Dec. 2016.

[49] P. K. Ray, S. R. Mohanty, and N. Kishor, "Proportional–integral controller based small-signal analysis of hybrid distributed generation systems," *Energy Convers. Manage.*, vol. 52, no. 4, pp. 1943–1954, Apr. 2011.

[50] A. Eid, S. Kamel, A. Korashy, and T. Khurshaid, "An enhanced artificial ecosystem-based optimization for optimal allocation of multiple distributed generations," *IEEE Access*, vol. 8, pp. 178493–178513, 2020.

[51] W. Zhao, L. Wang, and Z. Zhang, "Artificial ecosystem-based optimization: A novel nature-inspired meta-heuristic algorithm," *Neural Comput. Appl.*, vol. 32, no. 13, pp. 9383–9425, Sep. 2019.

[52] D. Yousri, T. S. Babu, S. Mirjalili, N. Rajasekar, and M. A. Elaziz, "A novel objective function with artificial ecosystem-based optimization for relieving the mismatching power loss of large-scale photovoltaic array," *Energy Convers. Manage.*, vol. 225, Dec. 2020, Art. no. 113385.

[53] F. A. Essa, M. A. Elaziz, and A. H. Elsheikh, "Prediction of power consumption and water productivity of seawater greenhouse system using random vector functional link network integrated with artificial ecosystem-based optimization," *Process Saf. Environ. Protection*, vol. 144, pp. 322–329, Dec. 2020.

[54] D. Saha and L. C. Saikia, "Automatic generation control of a multi-area CCGT-thermal power system using stochastic search optimised integral minus proportional derivative controller under restructured environment," *IET Gener., Transmiss. Distrib.*, vol. 11, no. 15, pp. 3801–3813, Oct. 2017, doi: 10.1049/iet-gtd.2016.1737.

EMAD M. AHMED (Senior Member, IEEE) received the B.Sc. and M.Sc. degrees from Aswan University, Egypt, in 2001 and 2006, respectively, and the Ph.D. degree from Kyushu University, Japan, in 2012.

He was with the Aswan Power Electronics Applications Research Center (APEARC), from 2012 to 2018. In 2018, he joined the Aswan Wireless Communication Research Center (AWCRC). He is currently an Associate Professor with the Department of Electrical Engineering, Faculty of Engineering, Aswan University. Moreover, he is on a leave in the Faculty of Engineering, Jouf University, Saudi Arabia. His current research interests include applied power electronics, especially in renewable energy applications, micro-grids, fault tolerant control, and battery management systems. He is a member of the IEEE Power Electronics Society (PELS), the IEEE Industrial Electronics Society (IES), and the IEEE Power and Energy Society (PES).

EMAD A. MOHAMED received the B.Sc. and M.Sc. degrees in electrical power engineering from Aswan University, Aswan, Egypt, in 2005 and 2013, respectively, and the Ph.D. degree in electrical power engineering from the Kyushu Institute of Technology, Japan, in 2019.

He was a Demonstrator with the Department of Electrical Engineering, Aswan Faculty of Engineering, Aswan University, from November 2007 to August 2013, and was an Assistant Lecturer, from 2013 to 2015. He was a Research Student with Kyushu University, Japan, from April to October 2015. He has been an Assistant Professor, since May 2019. He was in a Master Mobility Scholarship with the Faculté des Sciences et Technologies, Université de Lorraine, France – 1. The scholarship sponsored by FFEEBB ERASMUS MUNDUS. His current research interests include the applications of superconducting power devices, power system stability, and reliability and protection.

AHMED ELMELEGI received the B.Sc. and M.Sc. degrees in electrical power engineering from Aswan University, Aswan, Egypt, in 2005 and 2019, respectively. He has been with the Upper Egypt Electricity Distribution Company, Ministry of Electricity and Renewable Energy, Aswan, since 2007. His current research interests include applied power electronics in renewable energy applications, multi-level inverters, and micro-grids.

MOKHTAR ALY (Member, IEEE) received the B.Sc. and M.Sc. degrees in electrical engineering from Aswan University, Aswan, Egypt, in 2007, and 2012, respectively, and the Ph.D. degree from the Department of Electrical Engineering, Faculty of Information Science and Electrical Engineering, Kyushu University, Japan, in 2017.

In 2008, he joined as an Assistant Lecturer with the Department of Electrical Engineering, Aswan University, where he has been an Assistant Professor with the Faculty of Engineering, since 2017. He is currently a Postdoctoral Researcher with the Solar Energy Research Center (SERC-Chile), Universidad Técnica Federico Santa María, Chile. His current research interests include reliability of power electronics systems especially in renewable energy applications, multi-level inverters, fault tolerant control, electric vehicles, and light emitting diode (LED) lamp drivers. He is a member of the IEEE Power Electronics Society (PELS), the IEEE Industrial Electronics Society (IES), and the IEEE Power and Energy Society (PES).

OSAMA ELBAKSAWI received the B.Sc. degree (Hons.) in electrical engineering from the Faculty of Engineering, Suez Canal University, Egypt, in 1996, and the M.Sc. and Ph.D. degrees in power and electrical machines from Suez Canal University, in 2002 and 2009, respectively. From 2010 to 2014, he was an Assistant Professor in electrical engineering with the Faculty of Engineering, Port Said University. Since 2014, he has been an Assistant Professor with the College of Engineering, Jouf University. His research interests include power system and electrical machines, which can be classified into the following topics: control of power system, different optimization algorithms, load frequency control, micro-grid systems, drive systems and renewable energy conversion for PV, and wind systems.